

IN PRESS

Single Molecule FRET Reveals Pore Size and Opening Mechanism of Msc

Yong Wang (University of Illinois at Urbana-Champaign), Yanxin Liu (University of Illinois at Urbana-Champaign), Hannah DeBerg (University of Illinois at Urbana-Champaign), Takeshi Nomura (Victor Chang Cardiac Research Institute), Melinda Hoffman (University of Illinois at Urbana-Champaign), Paul Rohde (Victor Chang Cardiac Research Institute), Klaus Schulten (University of Illinois at Urbana-Champaign), Boris Martinac (Victor Chang Cardiac Research Institute), and Paul Selvin (University of Illinois, Urbana-Champaign)

Abstract:

The mechanosensitive channel of large conductance, which serves as a model system for mechanosensitive channels, has previously been crystallized in the closed form, but not in the open form. Ensemble measurements and electrophysiological sieving experiments show that the open-diameter of the channel pore is $>25\text{\AA}$, but the exact size and whether the conformational change follows a helix-tilt or barrel-stave model are unclear. Here we report measurements of the distance changes on liposome-reconstituted MscL transmembrane α -helices, using a "virtual sorting" single-molecule fluorescence energy transfer. We observed directly that the channel opens via the helix-tilt model and the open pore reaches 2.8 nm in diameter. In addition, based on the measurements, we developed a molecular dynamics model of the channel structure in the open state which confirms our direct observations.

<http://dx.doi.org/10.7554/elife.01834>

Please address questions to press@elifesciences.org. Details on how to cite *eLife* articles in news stories and our media policy are available at <http://www.elifesciences.org/news/for-the-press>. Articles published in eLife may be read on the journal site at <http://elife.elifesciences.org>.

To be notified of new content at *eLife*, sign up at <http://elife.elifesciences.org>.

1 Single Molecule FRET Reveals Pore Size and Opening Mechanism of
2 MscL
3
4
5
6

7 Yong Wang^{1,2}, Yanxin Liu^{1,2}, Hannah A. DeBerg^{1,2}, Takeshi Nomura³, Melinda Tonks Hoffman^{1,2}, Paul
8 R. Rohde³, Klaus Schulten^{1,2}, Boris Martinac^{3,4}, Paul R. Selvin^{1,2,5,*}
9

10
11
12
13
14 ¹Department of Physics, ²Center for the Physics of Living Cells, ⁵Center for Biophysics and
15 Computational Biology, University of Illinois at Urbana-Champaign, Urbana, IL, USA,
16 ³Molecular Cardiology and Biophysics Division, Victor Chang Cardiac Research Institute, ⁴University of
17 New South Wales, Sydney, Australia.
18
19
20
21

22 * To whom correspondence may be addressed:

23 Paul R. Selvin
24 Telephone: (217) 244-3371
25 Fax: (217) 333-4898
26 Email: selvin@illinois.edu
27
28

29 Running Title: smFRET study on the opening of MscL
30
31
32
33
34
35
36
37
38
39
40
41
42
43
44
45
46
47

48 ABSTRACT

49 The mechanosensitive channel of large conductance, which serves as a model system for
50 mechanosensitive channels, has previously been crystallized in the closed form, but not in the open form.
51 Ensemble measurements and electrophysiological sieving experiments show that the open-diameter of the
52 channel pore is $>25\text{\AA}$, but the exact size and whether the conformational change follows a helix-tilt or
53 barrel-stave model are unclear. Here we report measurements of the distance changes on liposome-
54 reconstituted MscL transmembrane α -helices, using a “virtual sorting” single-molecule fluorescence
55 energy transfer. We observed directly that the channel opens via the helix-tilt model and the open pore
56 reaches 2.8 nm in diameter. In addition, based on the measurements, we developed a molecular dynamics
57 model of the channel structure in the open state which confirms our direct observations.

58
59 Keywords: barrel-stave model / helix-tilt model / MscL

60
61 **Introduction**

62 Mechanosensitive (MS) channels are essential in both eukaryotes and prokaryotes (Haswell *et al*,
63 2011; Árnadóttir & Chalfie, 2010; Perozo, 2006). In eukaryotes, they are involved in diverse processes
64 such as embryonic development, touch, pain, hearing, lung growth, and muscle homeostasis (Chalfie,
65 2009; Hamill & Martinac, 2001; Árnadóttir & Chalfie, 2010). In bacteria, they are “safety valves”,
66 opening their pores to release the pressure to protect cells from hypo-osmotic shock (Booth & Blount,
67 2012). The rise in antibiotic resistance, and the crucial role MS channels play in bacterial adaptation,
68 makes it important to understand the MS channels as potentially new drug targets (Booth & Blount, 2012).

69 When high pressure (~ 10 mN/m) causes the bacterial mechanosensitive channel of large conductance
70 (MscL) to open, it forms a large, nonselective pore with a very high conductance (~ 3 nS) that is
71 permeable to various ions and small organic osmolytes. In 1998, MscL from *Mycobacterium tuberculosis*
72 in the closed state was crystallized by Rees and co-workers (Chang *et al*, 1998). They showed that MscL
73 is a pentamer made up of five identical subunits (Figure 1a-b). Each subunit consists of one cytoplasmic
74 α -helix (the CP domain) and two trans-membrane α -helices (the TM1 and TM2 helices), which extend
75 through the cell membrane and are joined by a periplasmic loop (Figure 1b). TM1 and TM2 are primarily
76 responsible for gating; it has been shown that complete deletion of the CP domain does not change the
77 gating parameters substantially (Anishkin *et al*, 2003).

78 Despite this progress, the open form of MscL has not been crystallized. This leaves two questions
79 unanswered: what is the exact size of the open pore of MscL, and how does the channel open? Several
80 techniques, e.g., permeation of organic ions (Cruickshank *et al*, 1997), Electron Paramagnetic Resonance
81 (EPR) (Perozo *et al*, 2002b, 2002a) and ensemble Fluorescence Resonance Energy Transfer (FRET)
82 (Corry *et al*, 2005b, 2010) have attempted to measure the pore size. However, systematic errors likely
83 result in an overestimation of (Cruickshank *et al*, 1997), an underestimation of (Corry *et al*, 2005b, 2010),
84 or an insensitivity to the requisite distances (Perozo *et al*, 2002a). For example, EPR was only able to
85 establish that the open pore is $> 25\text{\AA}$ (11). Ensemble FRET, which yielded some insightful results, is
86 potentially sensitive to larger distances (~ 80 - 100 \AA) (Roy *et al*, 2008). However, due to multiple labeling,
87 problems with protein clustering, and the need for Monte-Carlo simulations to extract distance
88 information, there was much variability and uncertainty in the results (Corry *et al*, 2005b, 2010, 2005a).

89 Another important question is how the MscL channels open, i.e. how the helices rearrange upon
90 channel activation (i.e., from the closed state to the open state). Currently, there exist two predominant
91 models for the opening of MscL: the barrel-stave model and the helix-tilt model (Figure 2) (Perozo, 2006).
92 The barrel-stave model involves motion of the transmembrane helix 1 (TM1) with the transmembrane
93 helix 2 (TM2) remaining stationary; the open-pore is lined by both TM1 and TM2 and the helices are
94 fairly vertical (where the membrane is horizontal). This model derives primarily from the number of
95 transmembrane helices and the large size of the open pore. In contrast, the helix-tilt model, which has

96 been proposed more recently (Sukharev *et al*, 2001a, 2001b; Betanzos *et al*, 2002), involves motion of
97 TM1 and TM2, with both swinging away from the pore upon channel opening and both helices tilting
98 toward the plane of membrane. Recent evidence from cysteine-crosslinking experiments, EPR
99 experiments, and ensemble FRET experiments, argue in favor of the helix-tilt model (Betanzos *et al*, 2002;
100 Perozo *et al*, 2002a; Corry *et al*, 2010).

101 In the present work, we focused on the transmembrane helices involved in the opening of MscL from
102 *Escherichia coli* (EcoMscL), using a single-molecule fluorescence resonance energy transfer (smFRET).
103 MscL channels were reconstituted in liposomes during smFRET measurements and thus the channels
104 were in their quasi-native environment. In addition, although MscL is a pentamer, we utilized
105 photobleaching to virtually sort out the population of molecules with a single donor and a single acceptor,
106 allowing us to make accurate smFRET measurements. It is the first time that smFRET has been applied to
107 liposome-reconstituted membrane proteins with more than three monomers. We measured movement of
108 three residues on TM1 (M42C, A27C, and I25C; Figure 1c) and three residues on TM2 (Y75C, Q80C and
109 V82C; Figure 1c), from which we determined not only the translational movements but also the tilting of
110 each helix. We observed the tilting of the helices in a model-free fashion, arguing strongly in favor of the
111 helix-tilt model. In addition, from the movement of the residue (I25C) right at the gating region, we
112 determined directly that the open pore reaches 2.8 nm in diameter. Lastly, we developed a molecular
113 dynamics model of the channel structure in the open state based on the smFRET results, while using the
114 crystal structure of the protein in the closed state as a reference. The model of the open structure satisfies
115 all the distance constraints measured from smFRET experiments. The developed open structure confirmed
116 that the pore size of the fully open channel is 2.8 nm in diameter, achieved via the helix-tilt opening
117 model.

118 119 **Results**

120
121 **FRET efficiencies.** Purified MscL mutants (Supplementary Figure 1) were labeled with Alexa Fluor 488
122 (AF488) and Alexa Fluor 568 (AF568) and reconstituted into ~ 50 nm liposomes made of 1-palmitoyl-2-
123 oleoyl-sn-glycero-3-phosphocholine (POPC) with 2% 1,2-dioleoyl-sn-glycero-3-phosphoethanolamine-N-
124 biotinyl (BPE) (Figure 1e). The liposomes were then immobilized on a glass coverslip, via biotin-avidin
125 interaction, for smFRET measurements (Figure 1e). To access the open state of the channels, 1-oleoyl-2-
126 hydroxy-sn-glycero-3-phosphocholine or lysophosphatidylcholine (LPC) of 25% molar ratio was added
127 (Perozo *et al*, 2002b, 2002a; Corry *et al*, 2005b, 2010) (Figure 1f) and incubated for > 10 minutes before
128 immobilization. Just before performing smFRET experiments, the fluorescence spectra of the samples (\pm
129 LPC) were recorded with excitation at 488 nm to confirm that the channels open up with LPC by
130 observing the shift in the FRET peaks. (The channel activity is also determined by observing the opening
131 of the channels upon application of negative pressure (suction) to the patch pipette. The labeled proteins
132 for patch-clamp experiments are from a different aliquot, although the same batch, of the labeled proteins
133 for smFRET experiments.) We emphasize that, although smFRET has been applied to study the
134 conformational changes of channels and transporters (Zhao *et al*, 2010, 2011; Akyuz *et al*, 2013; Choi *et al*,
135 2010), to our knowledge, it is the first time that smFRET has been used with channels reconstituted to
136 liposomes.

137 Via smFRET measurements, we observed fluorescence intensity traces with one or two
138 photobleaching steps (Supplementary Figure 2a-b). This is the expected result because MscL is a homo-
139 pentamer and the labeling of fluorophores is stochastic. The number of photobleaching steps tells the
140 number of fluorophores attached to a channel. Only the traces showing a single photobleaching step in
141 both the donor and acceptor channels, ensuring that only a single donor and/or acceptor fluorophore, were
142 included in the analysis (Supplementary Figure 2a). Donors were, in most cases, photobleached first,
143 resulting in simultaneous dropping of the fluorescence intensities in both donor and acceptor channels

144 (Supplementary Figure 2a-b). Subtraction of the intensities before and after photobleaching gives the
145 intensities of donor (I_D) and acceptor (I_A), which are used for the calculation of FRET efficiency. Note
146 that the intensities, I_D and I_A , automatically remove the direct excitation of acceptor (i.e. the leakage of
147 acceptor emission in the donor channel). However, the leakage of donor emission in the acceptor channel
148 is still present. To measure this leakage, MscL channels were labeled with donors-only and the leakage
149 coefficient (ℓ) was measured experimentally: $\ell = I_D^A/I_D^D \approx 0.09$, where I_D^A is the intensity of donor
150 emission in the acceptor channel and I_D^D is the intensity of donor emission in the donor channel.
151 Furthermore, to determine the actual FRET efficiency, another instrumental correction was made through
152 the correction factor γ , which accounts for the differences in quantum yield and detection efficiency
153 between the donor and the acceptor. It was calculated as the ratio of change in the acceptor intensity, ΔI_A ,
154 to the change in the donor intensity, ΔI_D , upon acceptor photobleaching: from the traces where the
155 acceptor photobleached first, we estimated the value $\gamma = \Delta I_A/\Delta I_D \approx 0.89 \pm 0.06$ (Supplementary Figure
156 2c).

157 We analyzed a few hundred traces (varying between 134 and 577 traces) with single photobleaching
158 steps in the absence and presence of LPC for each mutant (Figure 1c and Figure 3). Here we focus on the
159 mutant M42C for the sake of illustration. For the single photobleaching steps of M42C, 428 and 577
160 traces, in the absence and presence of LPC, respectively, were analyzed. The corrected FRET efficiencies
161 were calculated and their distribution was then plotted and fitted with Gaussians via maximum likelihood
162 estimates, shown in Figure 3a-b, while the number of Gaussians was determined according to the
163 corrected Akaike information criterion (AICc) and the Bayesian information criterion (BIC)
164 (Supplementary Table I) (Schwarz, 1978; Akaike, 1974; Sugiura, 1978). In the absence of LPC, we
165 observed three peaks at $E = 0.1, 0.28$ and 0.63 , respectively (Figure 3a). In the presence of LPC, the third
166 peak showing the highest FRET efficiency diminishes, leaving mainly two Gaussians ($E = 0.1$ and 0.23 ,
167 Figure 3b). This transition (i.e. the highest peak decreases and the lowest peak increases) is more obvious
168 when we plotted the difference between the normalized FRET distributions ($\sum P^X = 1$, where $X = +$ for
169 in the presence of LPC and $X = -$ for in the absence of LPC) under the two conditions, as shown in
170 Figure 3c: after adding 25% LPC, the peak at $E \sim 0.6$ went away but the fraction of the peak at $E \sim 0.1$
171 built up. Note that the highest peak at $E \sim 0.6$ does not completely disappear in the presence of 25% LPC,
172 which is consistent with Ref. (Perozo *et al*, 2002b).

173 In the absence of LPC, the existence of three peaks, rather than two peaks, can be explained by
174 considering the effect of tethering on the liposome. As the MscL channel is a homo-pentamer, we initially
175 expected two distances between donor and acceptor in each state (R_n and R_f in Figure 5a-b) and thus two
176 peaks for the distribution of FRET efficiency, assuming that all the channels are closed in the absence of
177 LPC. However, this assumption is not necessarily true, especially in our situation where liposomes are
178 immobilized and the proteins are responsive to membrane tension. It had been predicted by theories and
179 observed in experiments that immobilization of liposomes (or vesicles) results in significant membrane
180 tension and possibly rupture (Serro *et al*, 2012; Zhdanov *et al*, 2006; Chung *et al*, 2009). In our
181 experiments, the membrane tension is expected to be high, ~ 30 - 40 $k_B T$, due to the strong interaction
182 between BPE and the surface via biotin-neutravidin (Miyamoto & Kollman, 1993; Rico & Moy, 2007).
183 With such strong interaction, giant unilamellar vesicles ruptured spontaneously, as has been observed
184 experimentally (Chung *et al*, 2009). The consequence is that some of the MscL channels switch to the
185 open conformation upon the immobilization of the liposomes. (However, the fraction of open channels
186 might be different for different mutants even if the membrane tension is similar.) Therefore, the FRET
187 histogram for the no-LPC sample includes a mixture of closed and open MscL channels. This hypothesis
188 is supported by our results that show the number of open channels increases with the fraction of BPE
189 (Figure 3d; see Supplementary Information for details). In addition, a simple estimation based on the
190 crystal structure (Chang *et al*, 1998) and previously predicted open pore-size (Corry *et al*, 2010) gives that
191 R_n in the open state (R_{no}) is exactly the same as R_f in the closed state (R_{fc}), indicating that it is very likely

192 that the middle peak is an overlap of two peaks corresponding to R_{no} and R_{fc} . Furthermore, it has been
193 observed that $\leq 30\%$ of MscL are hexamers, instead of pentamers, in detergents such as n-Dodecyl- β -D-
194 maltopyranoside (DDM), used in the current study. This would tend to “smear” the middle peaks of
195 FRET in the absence of LPC. Therefore to be consistent and accurate, we always use the highest FRET
196 efficiency for the calculation of distance changes. On the other hand, we did find that all mutants give E_{fo}
197 measurements compatible (i.e., within error) with the final model (except that M42C is slightly off), as
198 shown in Supplementary Figure 9.

199 FRET between neighboring MscL channels on the same liposome had been a problem in previous
200 ensemble FRET experiments. To decrease the likelihood of its happening, and to effectively solve the
201 problem, we applied two strategies. First, we used 5% labeled channels together with 95% unlabeled ones
202 for reconstitution in liposomes. As a result, we had 16x lower molar ratio of labeled proteins (pentamers)
203 to lipids than that in the ensemble FRET experiments: 1:4000 vs. 1:250 (Corry *et al*, 2010, 2005b), greatly
204 reducing the likelihood of inter-molecular FRET. In addition, only traces showing a single photobleaching
205 step in both donor and acceptor channels were included in analysis, which helps further removing the
206 FRET between neighboring MscL channels in the analysis.

207 Another note is that we used maximum-likelihood estimation (MLE) (In Jae, 2003) for peak fitting.
208 This method was chosen particularly because it does not require binning the data before fitting. Although
209 there are mathematical ways for selection of “good” bin sizes (Shimazaki & Shinomoto, 2007), the
210 selection of bin size is, in practice, subjective, and the peaks derived can be affected with different bin
211 sizes. After MLE fitting, we then bin the data and plot the histograms for the sake of presentation purpose.
212 How the data is binned does not change the fitting parameters.

213
214 **Measurement of Förster radius, R_0 .** The Förster radius (R_0) for AF488 and AF568 is calculated by
215 means of $R_0 \propto (\kappa^2 Q_D)^{1/6}$ (Förster, 1948; Iqbal *et al*, 2008). Because κ^2 and Q_D , can be environmentally
216 sensitive, we measured the quantum yield and orientation factor for the fluorophores conjugated to each
217 and every channel mutant (Fery-Forgues & Lavabre, 1999; Lakowicz, 1999) (Figure 4). The quantum
218 yields of AF488 conjugated to various MscL mutants are summarized in Table I and Figure 4a, corrected
219 for polarization effects (Lakowicz, 1999; Fery-Forgues & Lavabre, 1999). It is noted that the fluorophores
220 used in the current study are mixtures of 5' and 6' isomers. However, it was expected that this will not
221 affect the results because 1) they have successfully been used in many smFRET studies (Granier *et al*,
222 2007; Jäger *et al*, 2006; Majumdar *et al*, 2007; Marras *et al*, 2002; Yin *et al*, 2005); 2) the chromophores
223 of the isomers are exactly the same while the only difference between the isomers lies in where the linker
224 of carbon-chain [(CH₂)₅NHCO] is attached; 3) we examined the molecular structures of the probe-isomers
225 and confirmed that the difference in molecular size is $< 5\%$ between isomers (see Supplementary Figure
226 7). The orientation factor κ^2 , was determined by measuring the anisotropy of the conjugated fluorophores
227 (Table I, Figure 4b and Supplementary Figure 3). The anisotropy of both donor and acceptor for most
228 residues is < 0.2 and therefore κ^2 , in fact, is close to 2/3 (Roy *et al*, 2008; Clegg, 1992; Andrews &
229 Demidov, 1999). Nonetheless, we calculated the maximum possible errors in R_0 due to anisotropic
230 orientation of the dyes (see Table I, Figure 4b and Supplementary Figure 3); the actual errors in R_0 should
231 be much smaller. Another source of error in R_0 lies in the measurements of Q_D , which were performed for
232 AF488-MscL in detergent (PBS + 1mM DDM), which was not exactly the same environment for
233 fluorophore-MscL conjugates in smFRET experiments (incorporated in liposomes in PBS), although the
234 buffer was kept the same. Furthermore, it is possible that the addition of LPC and the conformational
235 change of MscL changes Q_D as well, resulting in additional errors in R_0 and in the distances calculated
236 below.

237
238 **Estimation of residue movements.** We measured the change of FRET efficiency of MscL before and
239 after channel activation using smFRET. For example, for M42C, the FRET efficiency changed from 0.63

240 (closed state) to 0.23 (open state). We also determined experimentally the Förster radii ($R_0 = 5.5^{+0.4}_{-0.3}$ nm
241 for M42C). This permitted us to estimate the change in the distance between donors and acceptors from
242 the closed to open states (Figure 5), $\Delta R_n = R_{no} - R_{nc} = R_0 (E_{no}^{-1} - 1)^{-1} - R_0 (E_{nc}^{-1} - 1)^{-1}$ (≈ 1.7 nm for M42C).
243 We emphasize that some of the distances between fluorophores (R_{no} and R_{nc} in Supplementary Table II)
244 are indeed out of the sensitive range of EPR measurements, making FRET a more suitable technique in
245 this context.

246 We note that the finite size of probes ($r_p \sim 1.7$ nm) brings additional difficulties to converting FRET
247 measurements to estimation of distances: FRET results gave the distances between the chromophores of
248 donors and acceptors, which is different from the distances between the C_α atoms of residues of interest.
249 However, on the other hand, the *movement* of the residues (or the movement of the C_α atoms of the
250 residues) in the radial direction is the same as the *movement* of the chromophores assuming that the size
251 of the probes does not change (i.e. $\Delta r_p = 0$) upon channel opening (see Supplementary Information for
252 details). We also note that, although the five-fold symmetry is broken due to the binding of one donor and
253 one acceptor per pentamer, the geometric construction will not be affected.

254 As a result, we focus on the more relevant distance of interest: the movement of the residue away
255 from the pore center, Δr (Figure 5b), or the change of protein diameter measured from the residue, ΔD . (D
256 is the protein diameter defined by a specific residue, as shown in Figure 5a-b). Because of the five-fold
257 symmetry of the MscL channel, ΔD and Δr can be calculated readily according to $\Delta D = \Delta R_n / \sin(\pi/5) \approx$
258 2.8 nm, which yields $\Delta r = \Delta D / 2 \approx 1.4$ nm (for M42C). The Δr values of the residues are summarized in
259 Table I. These values are all above 2.5 nm, a lower bound predicted by EPR experiments (Perozo *et al*,
260 2002a), but are larger than ΔD values obtained from the previous ensemble FRET measurement: for
261 example, $\Delta D_{M42C} = 2.8$ nm (smFRET) *vs.* $\Delta D_{M42C} = 1.6$ nm (ensemble FRET) (Corry *et al*, 2010, 2005b).
262 We emphasize that the measurements of two more residues (I25C and A27C) in the current study were
263 also reported previously (Corry *et al*, 2010). Our results are close to the values in their simulations
264 ($\Delta D_{I25C} = 2.4$ *vs.* 2.5 nm; $\Delta D_{A27C} = 2.5$ *vs.* 2.6 nm) but differ significantly from the values measured
265 directly from ensemble FRET experiments ($\Delta D_{I25C} = 2.4$ *vs.* 0.2 nm). It should be noted that ensemble
266 experiments gave inconsistent measurements for $\Delta D_{I25C} = 0.2$ nm and $\Delta D_{A27C} = 2.9$ nm, although the two
267 residues are close. In contrast, smFRET results show that $\Delta D_{I25C} = 2.4$ nm is similar to $\Delta D_{A27C} = 2.5$ nm.
268 This clearly demonstrates the advantage of smFRET.

269 We note that fluorophores/linkers at different residues are likely to be constrained differently.
270 Furthermore, how they are constrained differently is not clear, partly due to the unavailability of the
271 crystal structure of EcoMscL. However, certain residues are in agreement between the EcoMscL and the
272 MtMscL (Perozo *et al*, 2001). Nevertheless, the distances between donors and acceptors are *not* good to
273 compare for different residues of EcoMscL. A more reasonable way is to compare the *changes* of
274 distances, i.e., the movements of residues.

275 The calculations above were performed with the assumption that EcoMscL are pentamers. However, a
276 caveat is that, in certain detergents, a small fraction of EcoMscL proteins present as hexamers, instead of
277 pentamers (Gandhi *et al*, 2011). To estimate the uncertainties due to a mixture of pentamers and hexamers,
278 we performed quantitative numerical simulations and showed that our results would be smaller than the
279 actual values by 7.5% in the presence of 30% hexamers in the sample (Supplementary Figure 1 and 4).

280 Because the size of both Alexa fluorophores is significant (~ 1.7 nm), it is possible that the attachment
281 of the fluorophores to MscL channel results in various effects on the protein and on the FRET
282 measurements. For example, the presence of the fluorophores might sterically hinder the conformational
283 change of the proteins and prevent them from opening or closing. On the other hand, the steric hindrance
284 might constrain the orientation of fluorophores, affect the relative orientation between the fluorophores
285 and therefore add more errors on the distances converted from FRET efficiencies. In addition, the
286 insertion of fluorophores to the protein might force the channel to be in a state different from the fully

287 closed state, resulting in the distance change measurement is underestimated. However, we would like
288 to emphasize that the expected effect is insignificant for the following reasons. First, if the insertion of
289 fluorophore would result in significant steric hindrance on the protein, it is expected that the labeling is
290 difficult (i.e., it takes much more effort for the fluorophores to be attached due to the steric hindrance). In
291 other words, it is expected that steric hindrance is not significant on the mutants that are labeled well.
292 More importantly, the channels after being labeled with AF488 and AF568 were confirmed to be
293 functional by both ensemble FRET experiments (by observing the shift in the FRET peak) and patch-
294 clamp measurements (by observing the opening of the channels upon application of negative pressure to
295 the patch pipette) as shown in Figure 6 and previous publications with the same fluorophores (Corry et al,
296 2010).

297
298 **Computational MscL opening model.** With smFRET, we measured the movements of three residues on
299 TM1 (M42C, A27C, and I25C) and three on TM2 (Y75C, Q80C and V82C) summarized in Table I and
300 Figure 5c-d. We observed directly and reliably for the first time, that both TM1 and TM2 swing away
301 from the pore, supporting the helix-tilt model. Note that, among the three residues on each helix, two sites
302 were very close to each other (A27C and I25C on TM1, Q80C and V82C on TM2). They were chosen
303 purposefully to be close; they served as consistency checks and confirmed that our smFRET
304 measurements are accurate (Table I). In addition, the top of both helices (periplasmic side, Figure 1b-c;
305 residues 42 on TM1 and 75 on TM2) moves further than the bottom (1.4 nm vs. 1.2 nm for TM1 and 2.0
306 nm vs. 1.4 nm for TM2), indicating that rotational tilting of the helices (toward the membrane plane) is
307 involved. We emphasize that it is the first *direct* (model-free) observation of both TM1 and TM2
308 swinging away from the pore center and of the tilting of the transmembrane helices. Therefore it is the
309 first *direct* observation in favor of the helix-tilt model.

310 To quantitatively investigate in detail how the MscL channel opens (i.e. how the helices move and
311 rotate upon opening), we developed a computational model for the open structure of the MscL, starting
312 from the crystal structure of MscL in the closed state (PDB: 2OAR) (Chang *et al*, 1998; Steinbacher *et al*,
313 2007) and employing the measured residue movements. For this purpose, we performed MD simulation
314 with distance constraints (Brünger *et al*, 1986; Trabuco *et al*, 2009) (i.e., a virtual spring, Supplementary
315 Figure 5) using NAMD 2.9 (Phillips *et al*, 2005). Although similar modeling attempts have been made by
316 Corry et al. (Corry *et al*, 2010) and Deplazes et al. (Deplazes *et al*, 2012) by using distance changes
317 measured from ensemble FRET, we would like to emphasize that all smFRET measurements were used
318 for the simulation while previously only a selected subset of ensemble data were used (as other data were
319 not consistent with the resultant model) (Corry *et al*, 2010). For each measured residue, ten virtual springs
320 were placed, five springs between the central carbon atom C_{α} of identical residues (highlighted green in
321 Supplementary Figure 5) from adjacent monomers (red springs in Supplementary Figure 5) and five
322 springs between the C_{α} of identical residues from non-adjacent monomers (yellow springs in
323 Supplementary Figure 5). The virtual springs were not applied to side chains because the flexibility of
324 side chains likely introduces errors under large forces in the modeling process. The equilibrium lengths of
325 the springs were chosen by adding the distance changes measured from smFRET to the equilibrium
326 distances seen in the closed state, thereby, opening the crystal structure of *Mycobacterium tuberculosis*
327 MscL (PDB: 2OAR) (Steinbacher *et al*, 2007; Chang *et al*, 1998; Perozo *et al*, 2001). In the simulation,
328 the virtual springs pushed corresponding residues from the distance in the closed state to the equilibrium
329 length in the open state. We note that the uncertainty due to the size of the FRET probes was minimized
330 by focusing on the change of the distances between the closed and open state, rather than absolute
331 distances as discussed in previous section.

332 We note several limitations in the modeling: as the spring constant was kept constant through the
333 simulations, resulting in a large force at beginning of the simulation, we applied both secondary structure
334 restraints (Trabuco *et al*, 2009) and symmetry restraints (Chan *et al*, 2011) to prevent structural distortion.

335 The secondary structure restraints prevents some subtle changes in the structure, such as kinks observed
336 previously in the upper part of TM1 in the open model of MscL (Deplazes *et al*, 2012). Therefore, we
337 limit our discussion of the open model to pore size and helix tilting. The membrane tension, which causes
338 membrane thinning, plays an important role in the MscL opening process (Corry *et al*, 2010; Louhivuori
339 *et al*, 2010; Deplazes *et al*, 2012). However, the restraint MD simulation cannot address the question of
340 how the channel is activated. For the simplicity of the modeling, membrane tension is not considered here.
341 We did observe that the membrane near the MscL becomes thinner during the channel opening process to
342 match with the flattening MscL (Supplementary Figure 6), confirming that a thinning membrane, likely
343 caused by tension, matches the open channel better.

344 The resulting open state structure of MscL is shown in Figure. 7b and d, and compared with the
345 crystal structure of MscL in the closed state (Figure 7a and c). The open structure satisfies all the distance
346 constraints measured in our smFRET experiments. In contrast, previous models based on ensemble FRET
347 measurements failed to be consistent with all experimental measurements (Corry *et al*, 2010). In the open
348 conformation, the pore is mainly lined by helices TM1 (indicated by blue arrows), consistent with the
349 helix-tilt model. In addition, it is observed that both TM1 and TM2 indeed tilt toward the membrane plane
350 (horizontal) upon channel activation. For example, the orientation of TM1 tilts from the green arrow
351 orientation (Figure 7c, closed state) to the yellow arrow orientation (Figure 7d, open state). The change in
352 tiling angle of the TM1 and TM2 helices is $\Delta\theta_1 \approx 27^\circ$ and $\Delta\theta_2 \approx 19^\circ$, respectively, where θ is the angle
353 between helix and the five-fold symmetry axis. The all-atom model and backbone model of the open state
354 resulting from the current study are provided in PDB format in SI.

355
356 **Measurement of pore size in the open conformation.** We used two independent methods to measure the
357 pore size of MscL in the open state. The first method is to measure the movements of the residues
358 forming the narrowest pore constriction of the channel, i.e. residues around I25 for *E. coli* MscL (Chang *et al*
359 *et al*, 1998; Perozo *et al*, 2001; Corry *et al*, 2010; Perozo *et al*, 2002a). However, this method, although
360 straightforward, has its limitations. It is likely that the function of the channel is affected by mutation and
361 labeling of (some of) the residues at the pore region. For example, the activation thresholds (P_a , defined as
362 the pressure at which the first channel opening was observed (Nomura *et al*, 2012)) of mutants G22C and
363 I24C are more than double the wild-type thresholds (Figure 6) and both ensemble and single molecule
364 FRET measurements of these mutants showed no change in the FRET efficiency after adding 25% LPC.
365 The effect of the point mutations near the pore on the electro-physiological properties of the channel can
366 be quantitatively explained by the closed and open structure of MscL As shown in Supplementary Figure
367 10, the residue G22 (A20 in *Mycobacterium tuberculosis* MscL) is very close to the pore and is facing the
368 pore. The residue V22 (V22 in *Mycobacterium tuberculosis* MscL) is also close to the pore and
369 sandwiched between helix 1 and neighboring helix 1. Mutating these two residues is likely to perturb the
370 channel function. On the other hand, the residue I25 is further from the pore than G22 and I24. The
371 mutation I25C is less likely effect the channel properties. Indeed the I25C mutation does not affect the
372 channel's gating parameters (Figure 6c-d). I25 is still close enough to the pore, making it a perfect
373 candidate for measuring pore size. Furthermore, among the three mutated residues shown in Figure 6, I25
374 (green) is the only one facing outward from the channel axis and accessible from the periphery of the
375 protein (see Supplementary Figure 10 B and D). We were able to determine the movement of residue
376 I25C (Corry *et al*, 2010); and measured that the residue I25 moves away from the pore center by $\Delta r = 1.2$
377 nm, indicating that the pore opens up by $\Delta D = 2.4$ nm in diameter. Taking into account that the pore
378 diameter in the closed state (Φ_{close}) is 0.4 nm (Chang *et al*, 1998), we conclude that the pore size in the
379 open state (Φ_{open}) is $\Phi_{\text{open}} = \Phi_{\text{close}} + \Delta D = 2.8$ nm, which agrees with previously reported values (Perozo *et al*
380 *et al*, 2002a; Corry *et al*, 2010).

381 The second method is based on the open state model of MscL constructed by means of molecular
382 dynamics. The surfaces of water molecules inside the channel were rendered (Figure 7e-f) using VMD

383 (Humphrey *et al*, 1996) and the narrowest constriction seen provided an estimate of the pore size. This
384 estimate accounts for all residues of the transmembrane domain and therefore is expected to be more
385 accurate than the estimate of the first method. Using this method we estimate that the pore size of the
386 MscL channel in the fully open state is 2.7 – 2.8 nm, which is consistent with the value from the first
387 method, 2.8 nm.

388 389 **Discussion**

390 We used a combination of experimental smFRET and computational modeling to study the
391 conformational change of MscL upon channel activation. It is the first time that single molecule FRET
392 has been applied to liposome-reconstituted membrane proteins with more than three monomers. We
393 measured the distance changes of multiple residues from the MscL transmembrane α -helices (TM1 and
394 TM2) during gating of the channel. For the first time, it is observed *directly* that both transmembrane
395 helices swing away from the pore center, with rotational tilting involved. The results argue clearly in
396 favor of the helix-tilt model. In addition, we developed by means of computational modeling a model of
397 the channel structure in the open state based on the smFRET results and the crystal structure of the protein
398 in the closed state as a reference. This model also confirms the helix-tilt model and yields a pore diameter
399 of 2.8 nm. The smFRET experiments carried out in the present study observe MscL channels dynamics in
400 lipid bilayers (liposomes) and not in detergents, which is a great advantage over crystallography that can
401 result in different oligomeric states like those seen in the tetrameric structure of *S. aureus* MscL (Liu *et al*,
402 2009). It is possible that the detergent used in purification caused some portion ($\leq 30\%$) of the MscL as
403 hexamers, instead of the assume pentamers. Nevertheless, our conclusion of the helix-tilt opening model
404 is independent of the percentage of hexameric structure. However, the exact value of the open pore
405 diameter would be slightly greater, 3.0 nm (30% hexamers), up to 3.3 nm (100% hexamers), still agreeing
406 with previously reported values (Perozo *et al*, 2002a; Corry *et al*, 2010; Sukharev *et al*, 2001b).

407 The current study focused on the closed and fully open state of MscL. The fully open state was
408 achieved by adding LPC to the liposomes (Perozo *et al*, 2002a, 2002b). However, the technique
409 introduced is not limited to these two states only. Single molecule FRET together with other techniques--
410 for example, with patch-clamping done simultaneously--can answer many more questions than a crystal
411 structure. For instance, it could probe the conformation of the channel during sub-conducting levels that
412 involve partial MscL openings, or probe sequence of movements of the individual channel domains
413 during opening of the channel.

414 415 **Materials and methods**

416
417 **Mutation, expression, purification and labeling of MscL.** The *E. coli* MscL gene (EcoMscL) was
418 cloned into plasmid pQE-32 (Qiagen) as the *Bam*HI-*Sal*I fragment, which also added a hexa-histidine tag
419 (his-tag) to the protein at the N-terminus. The protein was expressed in *E. coli* (M15 strain) (Qiagen) that
420 were lysed by sonication and purified from DDM solubilized membranes using TALON® Metal affinity
421 chromatography (Clontech Laboratories, Inc), followed by a further purification step using fast protein
422 liquid chromatography (FPLC; Superdex 200 10/300 GL column, GE Healthcare, Pittsburgh, US).
423 Purification was performed in the presence of 1 mM DDM.

424 The wild type of MscL protein does not contain any cysteine. To label the proteins with fluorescent
425 probes, MscL was mutated using site-directed mutagenesis such that a residue at the desired position was
426 replaced by a cysteine. Because the MscL protein is a homo-pentamer (Chang *et al*, 1998), this mutation
427 introduced five identical cysteine sites.

428 The protein with his-tag was then labeled with Alexa Fluor 488 (AF488) and/or Alexa Fluor 568
429 (AF568) maleimide, which specifically reacted with the introduced cysteines (Kim *et al*, 2008). Right
430 before labeling, proteins were reduced with 10 mM DTT for 30 minutes, followed by purification using

431 PD-10 desalting columns (GE Healthcare, Pittsburgh, US). We titrated the pentameric protein-to-
432 fluorophore molar ratio from 1:1 to 1:5 and used the molar ratio of 1:5 for labeling in all the experiments.
433 Under our labeling conditions, this ratio gave satisfying results such that most of the proteins are labeled
434 (averagely ~ 1.7 donors and ~ 1.3 acceptors per pentamer) and that many of proteins are attached by a
435 single donor and a single acceptor ($\sim 30\%$ of good traces show multiple donors and/or acceptors). Excess
436 fluorophores were then removed using PD-10 desalting columns. The sample was reduced with 10 mM
437 DTT before this purification step. A note to make is that the fluorophores (Alexa Fluor 488 maleimide
438 and Alexa Fluor 568 maleimide) come as mixtures of 5' and 6' isomers, which would potentially
439 complicate interpretation of smFRET data. However, we expect that the results would not be affected
440 because the exactly same fluorophores have been successfully used in many single molecule FRET
441 studies (Granier *et al*, 2007; Jäger *et al*, 2006; Majumdar *et al*, 2007; Marras *et al*, 2002; Yin *et al*, 2005).
442

443 **Reconstitution and opening of MscL in liposomes.** MscL channels were reconstituted into artificial
444 liposomes (~ 50 nm diameter), following the protocol described in Ref. (Perozo *et al*, 2002b, 2002a).
445 Liposomes were prepared by drying, rehydrating and extruding lipids through filters with ~ 50 nm pores.
446 The lipids used in all the measurements were a mixture of 1-palmitoyl-2-oleoyl-sn-glycero-3-
447 phosphocholine (POPC, Avanti polar lipids, Inc.) and 1,2-dioleoyl-sn-glycero-3-phosphoethanolamine-N-
448 biotinyl (BPE, Avanti polar lipids, Inc.) dissolved in chloroform at a molar ratio of POPC:BPE = 1000:20.
449 BPE was used for immobilization (see below). To incorporate MscL channels into the liposomes, a
450 mixture of unlabeled and labeled MscL proteins (5% labeled) was then reconstituted into the liposomes, at
451 a final volume of 1 ml, with a protein/lipid (molar) ratio of 1:200, resulting in a molar ratio of 1:4000 for
452 the labeled proteins to lipids. The liposomes were immobilized onto a glass coverslip. This
453 immobilization was achieved by biotin-avidin linkages between biotinylated-PEG molecules on the
454 surface to a neutravidin molecule, and then biotinylated lipids (BPE) in the liposomes (Roy *et al*, 2008).
455

456 To open the MscL channels in the liposomes, a conical lipid, 1-oleoyl-2-hydroxy-sn-glycero-3-
457 phosphocholine or lysophosphatidylcholine (LPC), was added to the liposomes, at a molar fraction of
458 25%. As LPC incorporates itself into the outer leaflet of a lipid bilayer, it introduces membrane tension,
459 changes the lipid pressure profile, and triggers the MscL to open (Perozo *et al*, 2002b, 2002a).

460 **Electrophysiological recording.** MscL protein purification and reconstitution into soybean azolectin
461 liposomes were described previously (Nomura *et al*, 2012). All results were obtained with
462 proteoliposomes at the protein: lipid ratio of 1:200 (w/w). Channel activities of the wild-type and mutant
463 MscL were examined in inside-out liposome patches using patch-clamp technique. Borosilicate glass
464 pipettes (Drammond Scientific Co, Broomall, PA) were pulled using a Narishige micropipette puller (PP-
465 83; Narishige, Tokyo, Japan). Pipettes with resistance of 2.5-4.9 M Ω were used for the patch-clamp
466 experiments. Pipette and bath solution contained 200 mM KCl, 40 mM MgCl₂, and 5 mM HEPES (pH
467 7.2 adjusted with KOH). The current was amplified with an Axopatch 200B amplifier (Molecular Devices,
468 Sunnyvale, CA), filtered at 2 kHz and data acquired at 5 kHz with a Digidata 1440A interface using
469 pCLAMP 10 acquisition software (Molecular Devices, Sunnyvale, CA) and stored for analysis. Negative
470 pressure (suction) was applied to the patch pipettes using a syringe and was monitored with a pressure
471 gauge (PM 015R, World Precision Instruments, Sarasota, FL).

472 **Selection of MscL with a single donor and a single acceptor.** Since the MscL channel is a homo-
473 pentamer (Chang *et al*, 1998) (or possibly homo-hexamer (Gandhi *et al*, 2011)), there is always a
474 distribution of various donor/acceptor combinations. To exclude signal from those channels having
475 multiple donors or multiple acceptors, the fluorescence intensity of single channels (and hence the step-
476 wise photobleaching) was monitored. Because multiple donors or acceptors have multiple "staircase"
477 photobleaching, these channels were simply not used. Only the traces with a clear single-step

478 photobleaching in both donor and acceptor channels were included in the analysis. Subtraction of the
479 intensities (averaged) before and after photobleaching gives the intensities of donor (I_D) and acceptor (I_A),
480 which are then used for FRET efficiency calculation as described below.

481
482 **Single molecule FRET measurement.** Single molecule FRET experiments were performed using total
483 internal reflection fluorescence microscopy (TIRFM) with a 1.45 NA 100X oil immersion objective (Roy
484 *et al*, 2008; Selvin & Taekjip, 2007). The fluorescence intensities were used to calculate the energy
485 transfer efficiency by the corrected FRET equation: $E = (I_A - \ell I_D) / (I_A + \gamma I_D)$: where E is the FRET
486 efficiency, ℓ represents leakage of donor signals in the acceptor channel, γ is the correction factor which
487 accounts for the differences in quantum yield and detection efficiency between the donor and the acceptor,
488 I_A and I_D represent the acceptor and donor intensities, respectively (Roy *et al*, 2008). Note that the direct
489 excitation of the acceptor by the donor excitation has been corrected automatically when getting the
490 acceptor intensity from the fluorescence traces. The distance between the donor and acceptor is given by
491 $R = R_0(E^{-1}-1)^{1/6}$, where R_0 is the Förster radius (Förster, 1948). The Förster radius, R_0 , given by $R_0 =$
492 $\left(\frac{0.529 \kappa^2 Q_D J(\lambda)}{N_A n^4}\right)^{1/6} \propto (\kappa^2 Q_D)^{1/6}$, and its error were measured experimentally by measuring the absorbance
493 and fluorescence spectra, quantum yield of the donor, AF488, ($Q_D = Q_{AF488}$) and anisotropy (A_a and A_d
494 which give the maximum possible error in κ^2) of the fluorescent probes conjugated to proteins.

495
496 **Measurement of quantum yield of AF488 conjugated to MscL.** The quantum yield of AF488
497 conjugated to MscL was measured using fluorescein in 0.1 M NaOH as a standard (Fery-Forgues &
498 Lavabre, 1999; Lakowicz, 1999) using the equation $Q_X = \frac{A_S}{A_X} \times \frac{F_X}{F_S} \times \left(\frac{n_X}{n_S}\right)^2 \times Q_S$, where Q is the quantum
499 yield, A is the absorbance at the excitation wavelength (470 nm); F is the area under the corrected
500 emission curve, and n is the refractive index of the solvent. Subscripts S and X refer to the standard
501 (fluorescein) and to the unknown (AF488), respectively. The spectra of absorbance and fluorescence of
502 AF488-MscL in PBS+DDM (1mM DDM) were measured using Agilent 8453 UV-Vis absorbance
503 spectrophotometer (Agilent technologies) and PC1 spectrofluorimeter (ISS, Inc.), respectively.

504
505 **Measurement of anisotropy of fluorophores conjugated to MscL.** In order to determine the maximum
506 error in the orientation factor, κ^2 , and therefore the error in R_0 , the anisotropy of the fluorophores
507 conjugated to MscL was measured. The fluorophores-protein conjugates were immobilized on a glass
508 coverslip which was covered with PEG (5% biotinylated), then a layer of neutravidin (Thermo Scientific),
509 followed by a layer of penta-his biotin conjugate (Qiagen). The emission of the fluorophores-protein
510 conjugates were split into two channels of polarization and used to calculate the anisotropy, $A = \frac{I_{\parallel} - I_{\perp}}{I_{\parallel} + 2I_{\perp}}$,
511 where I_{\parallel} is the fluorescence emission with polarization parallel to the excitation polarization and I_{\perp} is the
512 fluorescence emission with polarization perpendicular to the excitation polarization (Lakowicz, 1999).
513 Anisotropies were corrected for the intrinsic polarization properties of the microscope by calibrating to
514 known freely diffusing fluorophores. Anisotropies were also corrected for the high numerical aperture of
515 the objective. Then the maximum range of κ^2 was given by $\kappa^2_{\max} = 2/3(1+2.5A_d+2.5A_a)$ and $\kappa^2_{\min} = 2/3(1-$
516 $1.25A_d-1.25A_a)$ where A_d and A_a are the anisotropy of AF488 (donor) and AF568 (acceptor), respectively
517 (Cha *et al*, 1999; Dale *et al*, 1979).

518
519 **Modeling the MscL open structure through restraint molecular dynamics (MD) simulation.** Due to
520 lack of an *E. coli* MscL (EcoMscL) crystal structure, the simulation were performed using the structure of
521 MscL from *Mycobacterium tuberculosis* (MtMscL, PDB: 2OAR) (Steinbacher *et al*, 2007; Chang *et al*,
522 1998). The CP domain was truncated in the simulation because the complete deletion of the CP does not

523 change the gating parameters substantially (Anishkin *et al*, 2003). The residues to which the distance
524 constraints were applied, were shifted according to the sequence alignment in Ref. (Chang *et al*, 1998). A
525 spring constant of $0.2 \text{ kcal mol}^{-1} \text{ \AA}^{-2}$ was used for the virtual spring in the distance constrained simulation.
526 Both secondary structure restraints (Trabuco *et al*, 2009) and symmetry restraints (Chan *et al*, 2011) were
527 applied to prevent structural distortion under large force in the distance constrained simulation. Total
528 simulation time is 5 ns. A model of MscL in the open state was obtained at the end of the distance
529 constrained simulation, when the simulation satisfied all the distance constraints measured by means of
530 smFRET experiment. The restraint MD simulation procedure is similar to the one used previously (Corry
531 *et al*, 2010; Deplazes *et al*, 2012).

532 The simulation system was prepared by first imbedding the crystal structure of MscL (PDB: 2OAR)
533 (Steinbacher *et al*, 2007; Chang *et al*, 1998) into a membrane patch with 1727 POPC lipids. Solvent was
534 then added to both sides of the membrane, and the system was neutralized with 200 mM NaCl using
535 VMD (Humphrey *et al*, 1996). The final simulation system contained 1,137,413 atoms. The all-atom MD
536 simulations were performed using NAMD (Phillips *et al*, 2005) with the TIP3P model (Jorgensen *et al*,
537 1983) for explicit water and the CHARMM36 force field (Best *et al*, 2012). The simulation was
538 conducted in the NPT ensemble (constant pressure and temperature) with periodic boundary condition.
539 Constant temperature of 300 K was maintained using a Langevin thermostat with a damping coefficient of
540 1 ps^{-1} . A Nosé–Hoover Langevin piston barostat was used to maintain a constant pressure of 1 atm with a
541 period of 200.0 fs and damping timescale of 100.0 fs. The multiple time-stepping algorithm was
542 employed, with an integration time step of 2 fs, the short-range force being evaluated every time step, and
543 the long-range electrostatics every second time step. Non-bonded energies were calculated using particle
544 mesh Ewald full electrostatics and a smooth (10–12 Å) cutoff of the van der Waals energy.

546 **Acknowledgements**

547 This work was supported by NIH Grants R01 GM068625, R01 GM067887, U54 GM087519,
548 9P41GM10460, and the NSF Grants PHY0822613 and OCI-1053575, and NH&MRC Grant 635525. The
549 authors acknowledge supercomputer time on Stempede provided by the Texas Advanced Computing
550 Center (TACC) at The University of Texas at Austin through Extreme Science and Engineering
551 Discovery Environment (XSEDE) Grant MCA93S028. We thank Kai Wen Tseng for assistance with the
552 quantum yield measurements. We also thank Eduardo Perozo (U. of Chicago) for early work and for some
553 MscL plasmids.

555 **Author Contribution**

556 Y.W. and H.A.D. expressed and purified proteins. Y.W. performed single molecule FRET measurements.
557 Y.L. and K.S. performed molecular dynamics simulations. T.N. and B.M. performed electrophysiological
558 experiments. Y.W., Y.L., H.A.D. and T.N. analyzed data. M.T.H. and P.R.S. initiated the project. Y.W.,
559 Y.L. and P.R.S. wrote the paper with the help of all the other authors.

561 **Competing Financial Interests Statement**

562 The authors declare no competing financial interests.

571
572
573
574
575
576
577

References

- 578 Akaike H (1974) A new look at the statistical model identification. *IEEE Transactions on Automatic*
579 *Control* **19**: 716 – 723
580
- 581 Akyuz N, Altman RB, Blanchard SC & Boudker O (2013) Transport dynamics in a glutamate transporter
582 homologue. *Nature* **502**: 114–118
- 583 Andrews DL & Demidov AA (1999) Resonance Energy Transfer 1st ed. Wiley
- 584 Anishkin A, Gendel V, Sharifi NA, Chiang C-S, Shirinian L, Guy HR & Sukharev S (2003) On the
585 Conformation of the COOH-terminal Domain of the Large Mechanosensitive Channel MscL. *J*
586 *Gen Physiol* **121**: 227–244
- 587 Árnadóttir J & Chalfie M (2010) Eukaryotic Mechanosensitive Channels. *Annual Review of Biophysics* **39**:
588 111–137
- 589 Best RB, Zhu X, Shim J, Lopes PEM, Mittal J, Feig M & MacKerell AD (2012) Optimization of the
590 Additive CHARMM All-Atom Protein Force Field Targeting Improved Sampling of the Backbone
591 ϕ , ψ and Side-Chain χ_1 and χ_2 Dihedral Angles. *J. Chem. Theory Comput.* **8**: 3257–3273
- 592 Betanzos M, Chiang C-S, Guy HR & Sukharev S (2002) A large iris-like expansion of a
593 mechanosensitive channel protein induced by membrane tension. *Nature Structural & Molecular*
594 *Biology* **9**: 704–710
- 595 Booth IR & Blount P (2012) The MscS and MscL Families of Mechanosensitive Channels Act as
596 Microbial Emergency Release Valves. *J. Bacteriol.* **194**: 4802–4809
- 597 Brünger AT, Clore GM, Gronenborn AM & Karplus M (1986) Three-dimensional structure of proteins
598 determined by molecular dynamics with interproton distance restraints: application to crambin.
599 *PNAS* **83**: 3801–3805
- 600 Cha A, Snyder GE, Selvin PR & Bezanilla F (1999) Atomic scale movement of the voltage-sensing
601 region in a potassium channel measured via spectroscopy. *Nature* **402**: 809–813
- 602 Chalfie M (2009) Neurosensory mechanotransduction. *Nature Reviews Molecular Cell Biology* **10**: 44–52
- 603 Chan K-Y, Gumbart J, McGreevy R, Watermeyer JM, Sewell BT & Schulten K (2011) Symmetry-
604 Restrained Flexible Fitting for Symmetric EM Maps. *Structure* **19**: 1211–1218
- 605 Chang G, Spencer RH, Lee AT, Barclay MT & Rees DC (1998) Structure of the MscL Homolog from
606 *Mycobacterium tuberculosis*: A Gated Mechanosensitive Ion Channel. *Science* **282**: 2220 –2226

- 607 Choi UB, Strop P, Vrljic M, Chu S, Brunger AT & Wenginger KR (2010) Single-molecule FRET-derived
608 model of the synaptotagmin 1-SNARE fusion complex. *Nat Struct Mol Biol* **17**: 318–324
- 609 Chung M, Lowe RD, Chan Y-HM, Ganesan PV & Boxer SG (2009) DNA-tethered membranes formed
610 by giant vesicle rupture. *Journal of Structural Biology* **168**: 190–199
- 611 Clegg RM (1992) Fluorescence resonance energy transfer and nucleic acids. In *Methods in Enzymology*,
612 David M.J. Lilley JED (ed) pp 353–388. Academic Press Available at:
613 <http://www.sciencedirect.com/science/article/pii/007668799211020J> [Accessed February 26, 2013]
- 614 Corry B, Hurst AC, Pal P, Nomura T, Rigby P & Martinac B (2010) An improved open-channel structure
615 of MscL determined from FRET confocal microscopy and simulation. *The Journal of General*
616 *Physiology* **136**: 483–494
- 617 Corry B, Jayatilaka D & Rigby P (2005a) A Flexible Approach to the Calculation of Resonance Energy
618 Transfer Efficiency between Multiple Donors and Acceptors in Complex Geometries. *Biophys J*
619 **89**: 3822–3836
- 620 Corry B, Rigby P, Liu Z-W & Martinac B (2005b) Conformational Changes Involved in MscL Channel
621 Gating Measured using FRET Spectroscopy. *Biophys J* **89**: L49–L51
- 622 Cruickshank CC, Minchin RF, Le Dain AC & Martinac B (1997) Estimation of the pore size of the large-
623 conductance mechanosensitive ion channel of Escherichia coli. *Biophys J* **73**: 1925–1931
- 624 Dale RE, Eisinger J & Blumberg WE (1979) The orientational freedom of molecular probes. The
625 orientation factor in intramolecular energy transfer. *Biophys J* **26**: 161–193
- 626 Deplazes E, Louhivuori M, Jayatilaka D, Marrink SJ & Corry B (2012) Structural Investigation of MscL
627 Gating Using Experimental Data and Coarse Grained MD Simulations. *PLoS Comput Biol* **8**:
628 e1002683
- 629 Fery-Forgues S & Lavabre D (1999) Are Fluorescence Quantum Yields So Tricky to Measure? A
630 Demonstration Using Familiar Stationery Products. *J. Chem. Educ.* **76**: 1260
- 631 Förster T (1948) Zwischenmolekulare Energiewanderung und Fluoreszenz. *Annalen der Physik* **437**: 55–
632 75
- 633 Gandhi CS, Walton TA & Rees DC (2011) OCAM: A new tool for studying the oligomeric diversity of
634 MscL channels. *Protein Science* **20**: 313–326
- 635 Granier S, Kim S, Shafer AM, Ratnala VRP, Fung JJ, Zare RN & Kobilka B (2007) Structure and
636 Conformational Changes in the C-terminal Domain of the β 2-Adrenoceptor. *Journal of Biological*
637 *Chemistry* **282**: 13895–13905
- 638 Hamill OP & Martinac B (2001) Molecular Basis of Mechanotransduction in Living Cells. *Physiol Rev* **81**:
639 685–740
- 640 Haswell ES, Phillips R & Rees DC (2011) Mechanosensitive Channels: What Can They Do and How Do
641 They Do It? *Structure* **19**: 1356–1369

- 642 Humphrey W, Dalke A & Schulten K (1996) VMD: visual molecular dynamics. *J Mol Graph* **14**: 33–38,
643 27–28
- 644 In Jae M (2003) Tutorial on maximum likelihood estimation. *Journal of Mathematical Psychology* **47**:
645 90–100
- 646 Iqbal A, Arslan S, Okumus B, Wilson TJ, Giraud G, Norman DG, Ha T & Lilley DMJ (2008) Orientation
647 dependence in fluorescent energy transfer between Cy3 and Cy5 terminally attached to double-
648 stranded nucleic acids. *Proceedings of the National Academy of Sciences* **105**: 11176–11181
- 649 Jäger M, Nir E & Weiss S (2006) Site-specific labeling of proteins for single-molecule FRET by
650 combining chemical and enzymatic modification. *Protein Science* **15**: 640–646
- 651 Jorgensen WL, Chandrasekhar J, Madura JD, Impey RW & Klein ML (1983) Comparison of simple
652 potential functions for simulating liquid water. *The Journal of Chemical Physics* **79**: 926–935
- 653 Kim Y, Ho SO, Gassman NR, Korlann Y, Landorf EV, Collart FR & Weiss S (2008) Efficient Site-
654 Specific Labeling of Proteins via Cysteines. *Bioconjugate Chem.* **19**: 786–791
- 655 Lakowicz JR (1999) Principles of Fluorescence Spectroscopy 2nd ed. Springer
- 656 Liu Z, Gandhi CS & Rees DC (2009) Structure of a tetrameric MscL in an expanded intermediate state.
657 *Nature* **461**: 120–124
- 658 Louhivuori M, Risselada HJ, Giessen E van der & Marrink SJ (2010) Release of content through
659 mechano-sensitive gates in pressurized liposomes. *PNAS* **107**: 19856–19860
- 660 Majumdar DS, Smirnova I, Kasho V, Nir E, Kong X, Weiss S & Kaback HR (2007) Single-molecule
661 FRET reveals sugar-induced conformational dynamics in LacY. *PNAS* **104**: 12640–12645
- 662 Marras SAE, Kramer FR & Tyagi S (2002) Efficiencies of fluorescence resonance energy transfer and
663 contact-mediated quenching in oligonucleotide probes. *Nucl. Acids Res.* **30**: e122–e122
- 664 Miyamoto S & Kollman PA (1993) Absolute and relative binding free energy calculations of the
665 interaction of biotin and its analogs with streptavidin using molecular dynamics/free energy
666 perturbation approaches. *Proteins: Structure, Function, and Bioinformatics* **16**: 226–245
- 667 Nomura T, Cranfield CG, Deplazes E, Owen DM, Macmillan A, Battle AR, Constantine M, Sokabe M &
668 Martinac B (2012) Differential effects of lipids and lyso-lipids on the mechanosensitivity of the
669 mechanosensitive channels MscL and MscS. *PNAS* **109**: 8770–8775
- 670 Perozo E (2006) Gating prokaryotic mechanosensitive channels. *Nat Rev Mol Cell Biol* **7**: 109–119
- 671 Perozo E, Cortes DM, Sompornpisut P, Kloda A & Martinac B (2002a) Open channel structure of MscL
672 and the gating mechanism of mechanosensitive channels. *Nature* **418**: 942–948
- 673 Perozo E, Kloda A, Cortes DM & Martinac B (2001) Site-Directed Spin-Labeling Analysis of
674 Reconstituted MscL in the Closed State. *The Journal of General Physiology* **118**: 193–206

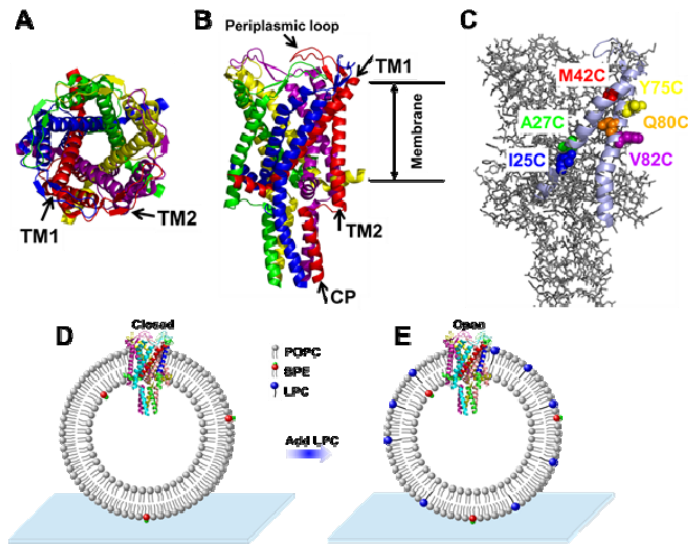
- 675 Perozo E, Kloda A, Cortes DM & Martinac B (2002b) Physical principles underlying the transduction of
676 bilayer deformation forces during mechanosensitive channel gating. *Nat Struct Mol Biol* **9**: 696–
677 703
- 678 Phillips JC, Braun R, Wang W, Gumbart J, Tajkhorshid E, Villa E, Chipot C, Skeel RD, Kalé L &
679 Schulten K (2005) Scalable Molecular Dynamics with NAMD. *J Comput Chem* **26**: 1781–1802
- 680 Rico F & Moy VT (2007) Energy landscape roughness of the streptavidin–biotin interaction. *Journal of*
681 *Molecular Recognition* **20**: 495–501
- 682 Roy R, Hohng S & Ha T (2008) A practical guide to single-molecule FRET. *Nat Meth* **5**: 507–516
- 683 Schwarz G (1978) Estimating the Dimension of a Model. *The Annals of Statistics* **6**: 461–464
- 684 Selvin PR & Taekjip H eds. (2007) Single-Molecule Techniques: A Laboratory Manual 1st ed. Cold
685 Spring Harbor Laboratory Press
- 686 Serro AP, Carapeto A, Paiva G, Farinha JPS, Colaço R & Saramago B (2012) Formation of an intact
687 liposome layer adsorbed on oxidized gold confirmed by three complementary techniques: QCM-D,
688 AFM and confocal fluorescence microscopy. *Surface and Interface Analysis* **44**: 426–433
- 689 Shimazaki H & Shinomoto S (2007) A Method for Selecting the Bin Size of a Time Histogram. *Neural*
690 *Computation* **19**: 1503–1527
- 691 Steinbacher S, Bass R, Strop P & Rees DC (2007) Structures of the Prokaryotic Mechanosensitive
692 Channels MscL and MscS. In *Mechanosensitive Ion Channels, Part A* pp 1–24. Academic Press
693 Available at: <http://www.sciencedirect.com/science/article/pii/S1063582306580019> [Accessed
694 August 30, 2012]
- 695 Sugiura N (1978) Further analysts of the data by akaike' s information criterion and the finite corrections.
696 *Communications in Statistics - Theory and Methods* **7**: 13–26
- 697 Sukharev S, Betanzos M, Chiang C-S & Guy HR (2001a) The gating mechanism of the large
698 mechanosensitive channel MscL. *Nature* **409**: 720–724
- 699 Sukharev S, Durell SR & Guy HR (2001b) Structural models of the MscL gating mechanism. *Biophys J*
700 **81**: 917–936
- 701 Trabuco LG, Villa E, Schreiner E, Harrison CB & Schulten K (2009) Molecular dynamics flexible fitting:
702 A practical guide to combine cryo-electron microscopy and X-ray crystallography. *Methods* **49**:
703 174–180
- 704 Yin J, Lin AJ, Buckett PD, Wessling-Resnick M, Golan DE & Walsh CT (2005) Single-Cell FRET
705 Imaging of Transferrin Receptor Trafficking Dynamics by Sfp-Catalyzed, Site-Specific Protein
706 Labeling. *Chemistry & Biology* **12**: 999–1006
- 707 Zhao Y, Terry D, Shi L, Weinstein H, Blanchard SC & Javitch JA (2010) Single-molecule dynamics of
708 gating in a neurotransmitter transporter homologue. *Nature* **465**: 188–193

709 Zhao Y, Terry DS, Shi L, Quick M, Weinstein H, Blanchard SC & Javitch JA (2011) Substrate-modulated
 710 gating dynamics in a Na⁺-coupled neurotransmitter transporter homologue. *Nature* **474**: 109–113

711 Zhdanov VP, Dimitrievski K & Kasemo B (2006) Adsorption and Spontaneous Rupture of Vesicles
 712 Composed of Two Types of Lipids. *Langmuir* **22**: 3477–3480

713
 714
 715

Figures and Figure Legends



716
 717
 718
 719
 720
 721
 722
 723
 724
 725
 726
 727

Figure 1. Cartoon representation of the structure of MscL in the closed conformation in the (a) top view and (b) side view (PDB ID: 2OAR (Chang *et al*, 1998; Steinbacher *et al*, 2007)), and scheme of single molecule FRET setup. MscL is a homo-pentamer consisting of five identical subunits. Each subunit consists of one cytoplasmic α -helix (CP) and two trans-membrane α -helices (TM1 and TM2), which extend through the cell membrane and are joined by a periplasmic loop (Chang *et al*, 1998). (c) Residues measured using smFRET. Three residues on each of the transmembrane helices (M42C, A27C and I25C on TM1; Y75C, Q80C and V82C on TM2) were chosen. Note that no residues on the CP were chosen because the complete deletion of the CP does not change the gating parameters substantially (Anishkin *et al*, 2003). (d) Labeled MscL proteins were reconstituted into liposomes, which were then immobilized on a coverslip and used for smFRET experiments. (e) The addition of LPC traps the protein in the open conformation (Perozo *et al*, 2002b).

728
729
730
731
732
733
734
735

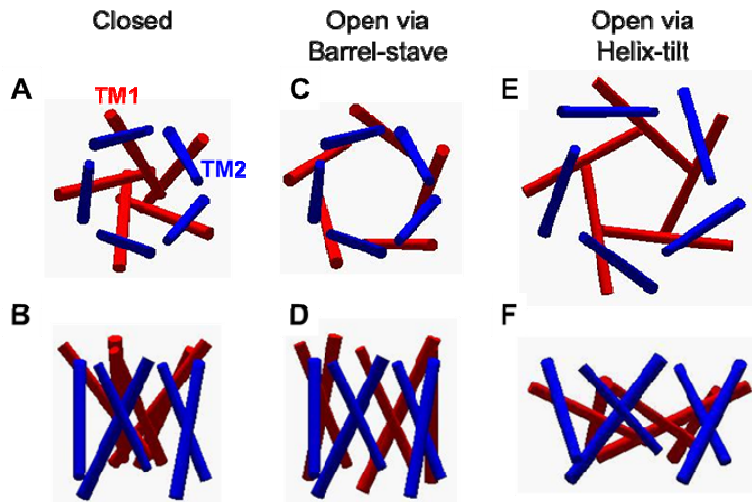


Figure 2. The opening models for MscL. The MscL opens from (a, b) the closed state, to (c, d) the open state via the barrel-stave model or (e, f) the open state via the helix-tilt model. The top figures (a, c, e) are top views and the bottom figures (b, d, f) are the side views. TM1 helices are shown in red while TM2 in blue. In the barrel-stave model (c, d), TM1 swings away from the pore center but TM2 remains stationary upon channel activation, generating an open pore lined by both TM1 and TM2 and the helices are more parallel to the membrane normal than the membrane plane. In the helix-tilt model (e, f), both TM1 and TM2 swing away from the symmetry axis and both helices tilt toward the plane of membrane.

736
737
738
739

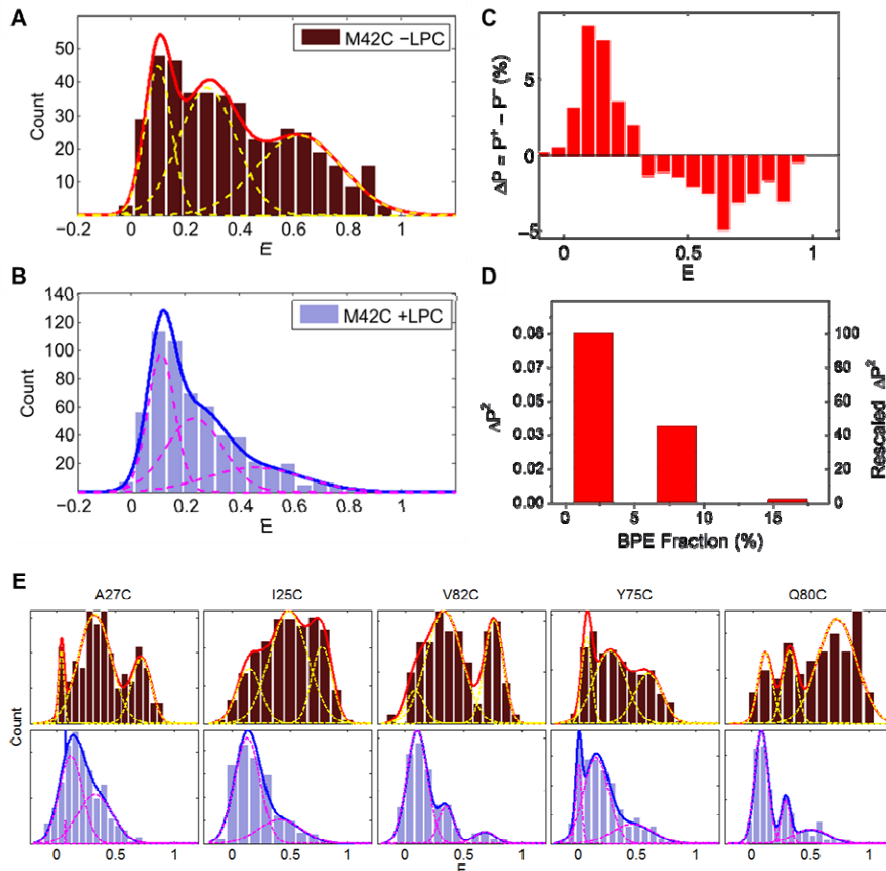
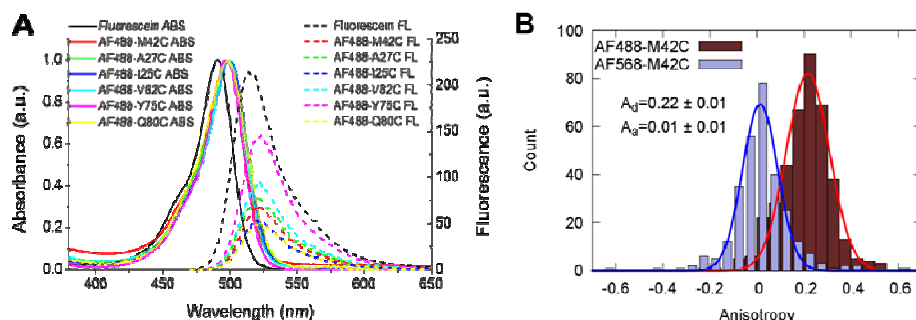
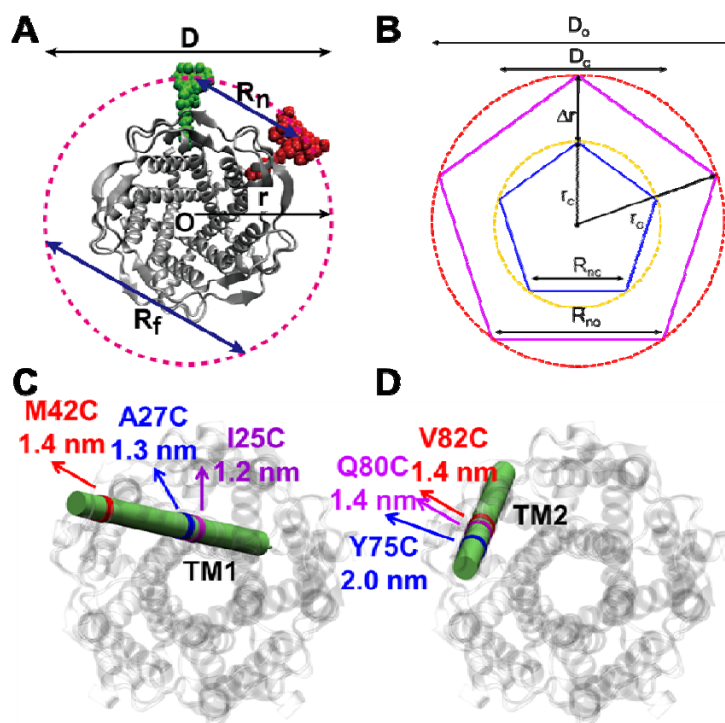


Figure 3. Single molecule FRET results for MscL M42C. The distribution of FRET efficiency of M42C in the (a) absence and (b) presence of LPC were plotted and fitted with Gaussians. (c) The difference between the normalized FRET distributions under the two conditions (\pm LPC), ΔP , emphasizes

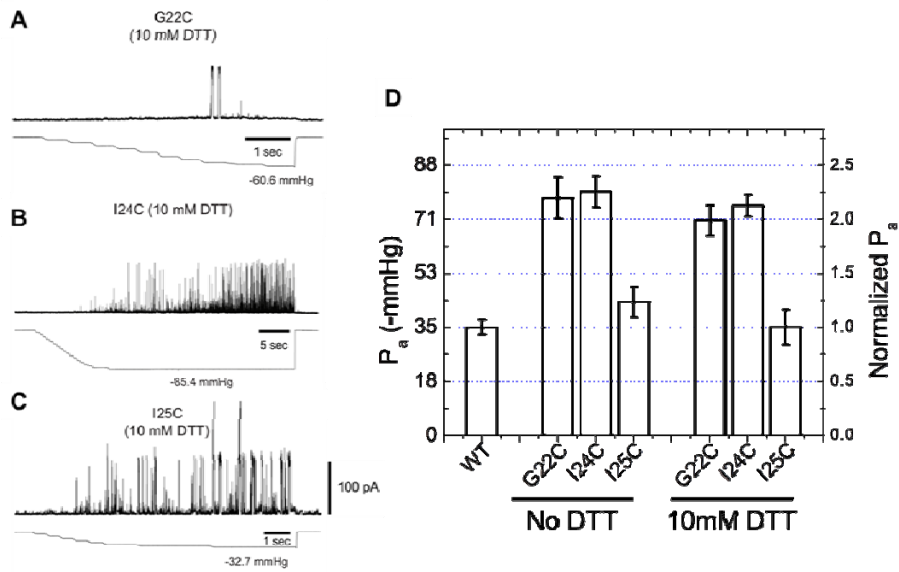
740 the diminishing of the third peak at $E \sim 0.6$ after adding LPC. (d) The variance between the normalized
 741 FRET distributions under the two conditions (\pm LPC), ΔP^2 , decreases as the fraction of BPE in the
 742 liposomes is increased from 2% to 16%. (e) Histograms of FRET efficiencies in the absence (top row, -
 743 LPC) and presence (bottom row, +LPC) of LPC for the other five residues (I25C, A27C, Y75C, Q80C,
 744 and V82C) that were measured in the current study.



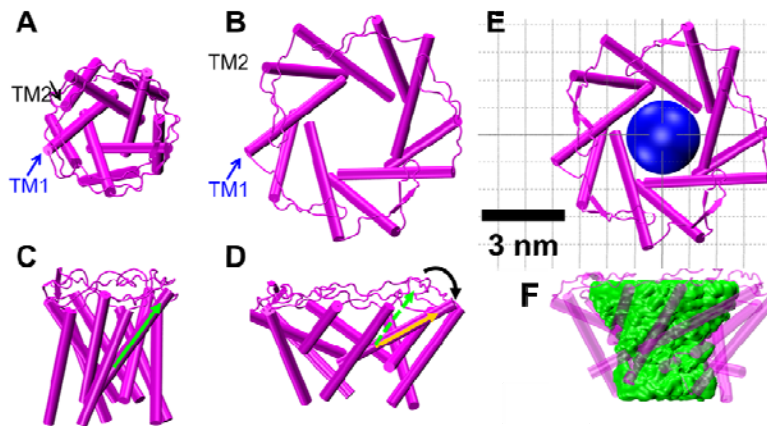
745 **Figure 4. Measurement of R_0 .** (a) Absorbance and fluorescence spectra of AF488-MscL and fluorescein
 746 (as a standard), used to determine the quantum yield of AF488 conjugated to MscL mutants. (b)
 747 Anisotropy of AF488 and AF568 conjugated to MscL mutant (M42C), corrected for the intrinsic
 748 polarization properties of the microscope, and for the high numerical aperture of the objective.
 749
 750



751 **Figure 5. Movement of residues.** (a) Each residue (highlighted in green) defines a circumcircle (dashed
 752 red circle) of radius r (or diameter D , where D , as shown, is D_{closed} , although upon opening would be
 753 D_{open}), centered at the pore center (O). Upon channel activation, the protein expands (radius changes from
 754 r_{close} to r_{open}), or equivalently, the residue moves by $\Delta r = r_{open} - r_{close}$, measured from the pore center (O).
 755 (b) Sketch of MscL from closed state (blue pentagon) to open state (purple pentagon). The residue of
 756 interest (vertices of the pentagons) moves Δr from the pore center. (c, d) Translational movements (Δr) of
 757 residues on TM1 and TM2 measured via smFRET. All the residues move away from the pore center,
 758 arguing in favor of the helix-tilt model.
 759



760
 761 **Figure 6. Activation thresholds, P_a , of MscL mutants at the proximity of the narrowest pore**
 762 **constriction.** The activation thresholds were determined by electro-physiological recordings by patch-
 763 clamping without and with 10 mM DTT. Three recordings in the presence of DTT are shown as examples:
 764 (a) G22C, (b) I24C, and (c) I25C. (d) Comparison of the mutants with the wild type (WT) shows that the
 765 thresholds for mutants G22C and I24C are more than twice higher than the wild type, indicating the
 766 function of the channel was affected by the mutations. This was also observed via ensemble and single
 767 molecule FRET experiments. However, the mutation I25C does not affect the gating parameter
 768 substantially.



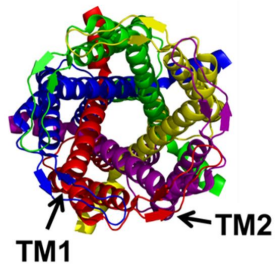
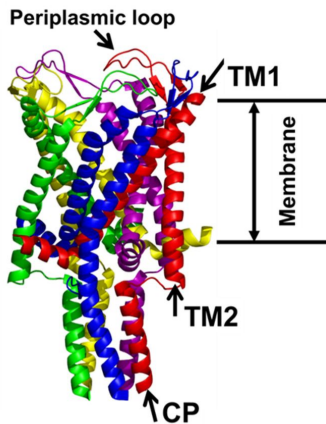
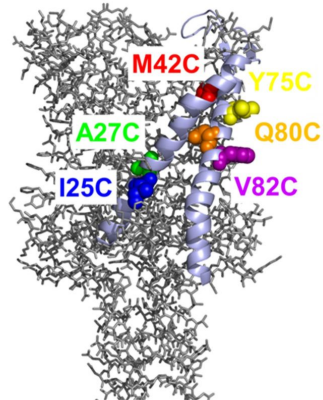
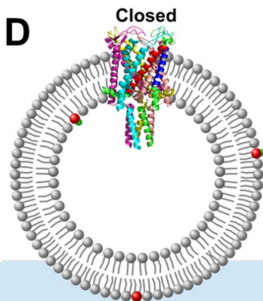
769
 770 **Figure 7. Model of the MscL structure in the open conformation.** (a, c) The crystal structure of MscL
 771 in the closed state is shown for comparison (PDB: 2OAR (Chang *et al.*, 1998; Steinbacher *et al.*, 2007)). (b,
 772 d) The structure of MscL in the open state was developed based on the smFRET measurements, satisfying
 773 all the distance constraints measured from smFRET experiments. In the open conformation, the pore is
 774 mainly lined by TM1 (indicated by blue arrows), consistent with the helix-tilt model. In addition, both
 775 TM1 and TM2 tilt toward the membrane plane (horizontal) upon channel activation, which is emphasized
 776 by the green and yellow arrows in the side views. The green arrows show the orientation of TM1 in the
 777 closed state while the yellow arrow indicated the orientation of TM1 in the open state. The angle between
 778 the two arrows is 27° . (e) A sphere with a diameter of 2.7 nm (blue) is shown in the MscL channel in the
 779 top view. (f) The surfaces of water molecules (green) inside the tunnel of MscL (magenta) are drawn and
 780 the narrowest constriction is $\sim 2.7 - 2.8$ nm.

781
 782
 783
 784
 785
 786
 787
 788
 789
 790

Table I. Measurements of smFRET experiments. Q_d is the quantum yield of donor (AF488) after conjugation to each MscL mutant. A_d and A_a are the anisotropy of donor (AF488) and acceptor (AF568) after conjugation, respectively. R_0 is the Förster radius. E_{nc} and E_{no} are the FRET efficiencies in the closed and open states, respectively. ΔR is the change in the distances between donor and acceptor ($\Delta R_n = R_{no} - R_{nc}$, Figure 5a-b). ΔD is the change of the protein diameter ($\Delta D = D_{open} - D_{close}$). Δr is the translational movement of the residue, measured from the pore center, $\Delta r = \Delta D / 2$. Note that the errors shown in the table are the maximum possible errors due to anisotropic orientation of the dyes. The actual errors are expected to be much smaller.

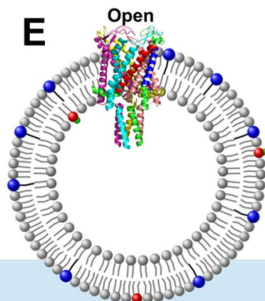
Residue	Helix	Q_d	A_d	A_a	R_0 (nm)	E_{nc}	E_{no}	ΔR_n (nm)	Δr (nm)	ΔD (nm)
42	TM1	0.33	0.22	0.01	$5.5^{+0.4}_{-0.3}$	0.63	0.23	$1.7^{+0.7}_{-0.5}$	$1.4^{+0.6}_{-0.4}$	$2.8^{+1.1}_{-0.8}$
27	TM1	0.28	0.12	0.09	$5.3^{+0.4}_{-0.3}$	0.72	0.33	$1.5^{+0.6}_{-0.4}$	$1.3^{+0.5}_{-0.3}$	$2.5^{+0.9}_{-0.6}$
25	TM1	0.42	0.19	0.06	$5.7^{+0.5}_{-0.4}$	0.78	0.42	$1.4^{+0.6}_{-0.5}$	$1.2^{+0.6}_{-0.4}$	$2.4^{+1.1}_{-0.8}$
75	TM2	0.62	0.19	0.11	$5.6^{+0.6}_{-0.5}$	0.60	0.16	$2.4^{+1.0}_{-0.7}$	$2.0^{+0.8}_{-0.6}$	$4.0^{+1.6}_{-1.2}$
80	TM2	0.22	0.18	0.09	$5.1^{+0.5}_{-0.3}$	0.72	0.29	$1.6^{+0.7}_{-0.4}$	$1.4^{+0.6}_{-0.4}$	$2.7^{+1.1}_{-0.8}$
82	TM2	0.39	0.24	0.13	$6.1^{+0.7}_{-0.6}$	0.76	0.35	$1.6^{+0.9}_{-0.8}$	$1.4^{+0.8}_{-0.6}$	$2.7^{+1.5}_{-1.3}$

791

A**B****C****D**

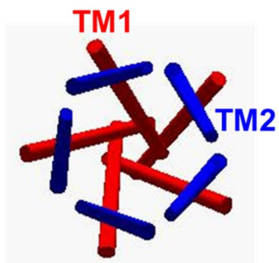
○ POPC
 ● BPE
 ● LPC

Add LPC

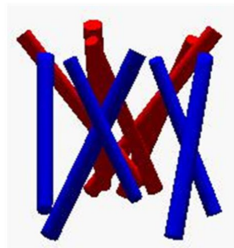
E

Closed

A

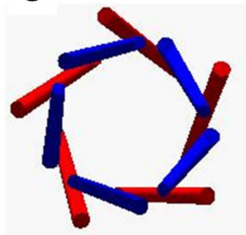


B

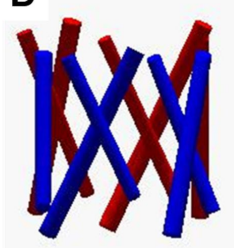


Open via
Barrel-stave

C

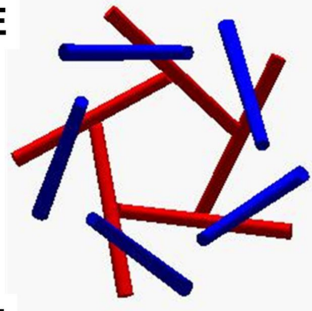


D



Open via
Helix-tilt

E



F

